

Constraints of internal symmetry on the non-Hermitian skin effect and bidirectional skin effect under the action of the Hermitian conjugate of time-reversal symmetry

Shu-Xuan Wang*

Guangdong Provincial Key Laboratory of Magnetoelectric Physics and Devices,
School of Physics, Sun Yat-sen University, Guangzhou 510275, China

(Dated: February 16, 2024)

Non-Hermitian skin effect is a basic phenomenon in non-Hermitian systems, which means that an extensive number of eigenstates can be localized at the boundary. In this Letter, we systematically investigate the constraints from all internal symmetries on the non-Hermitian skin effect in arbitrary dimensions. By adopting the powerful Amoeba formulation, we build a generic correspondence between the various internal symmetries and the behavior of the non-Hermitian skin effect. Notably, we find that, for non-Hermitian systems with the Hermitian conjugate symmetry of time-reversal symmetry (TRS^\dagger), the eigenstates can simultaneously localize at opposite boundaries, which is beyond the Amoeba formulation and we dub the phenomenon *bidirectional skin effect*. Our work provides an overall perspective from the internal symmetry to the non-Hermitian skin effect.

Introduction— Hermiticity of Hamiltonian is a fundamental assumption for closed systems. Once a system has gain and loss, it can effectively be described by a non-Hermitian Hamiltonian[1–5]. In recent years, non-Hermitian systems have attracted very active studies[5–15], accompanying with the discovery of many novel phenomena, such as exceptional points[5, 16–26], non-Hermitian PT symmetry breaking[27, 28], edge burst[29–32], etc. In experiment, such non-Hermitian systems can be realized in photonic crystals[33, 34], ultracold atoms[35, 36] and acoustic cavities[37, 38]. One particularly intriguing phenomenon in non-Hermitian systems is the so-called non-Hermitian skin effect (NHSE)[8, 10, 36, 39–51], which refers to the presence of abundant bulk states at the boundary. As is known, for Hermitian systems under open boundary conditions (OBC) the wave functions of bulk states are always extended, and only topological states are sharply localized at the boundary. The spectra of a Hermitian system under OBC and periodic boundary conditions (PBC) are almost the same except for the topological modes. Thus, the rise of NHSE in a non-Hermitian system implies that the wave functions and spectra under OBC are drastically different from those under PBC. For one-dimensional (1D) non-Hermitian systems, both the wave functions and the spectra of bulk states under OBC can be well described by the non-Bloch band theory[10, 15]. For dimensions higher than 1D, building non-Bloch band theory turns out to be quite challenging, and only very recently it has been uncovered that the Amoeba formulation could provide a general framework for studying higher-dimensional NHSE[50–52].

Since the Hamiltonian is no longer an Hermitian operator, there are seven rather than three internal symmetries for non-Hermitian systems[6]. Similar to Hermitian systems, an internal symmetry will put certain constraint on the spectra of non-Hermitian systems. Take the particle-hole symmetry as an example. If the system has an eigenstate with eigenenergy E , then there must be another

eigenstate at $-E$ [36]. Notably, the internal symmetry also puts constraints on the NHSE. Some previous works have shown that the TRS^\dagger can result in a class of \mathbb{Z}_2 skin effect in 1D non-Hermitian systems[11, 41], while the particle-hole symmetry in arbitrary dimensions enforces two particle-hole partner skin modes to localize at opposite boundaries. Although those case-by-case works have revealed the existence of nontrivial interplay between the internal symmetry and the NHSE, the generic relation between them remains to be established.

In this Letter, we systematically investigate the influence of all seven internal symmetries on the NHSE through the Amoeba formulation. By analytically calculating the transformation of winding number associated with the Ronkin function, we determine the generic relation between the internal symmetry and the NHSE in arbitrary dimensions. Furthermore, we note that the skin modes in a non-Hermitian system with TRS^\dagger can simultaneously be localized at opposite boundaries, a phenomenon that we dub as *bidirectional skin effect*. Notably, we find that this phenomenon is beyond the description of the Amoeba formulation, but can be captured by the TRS^\dagger winding numbers defined by us.

Internal symmetry of non-Hermitian systems— Owing to the lift of the constraint from hermiticity, the type of internal symmetry is enriched in non-Hermitian systems. The seven internal symmetries for non-Hermitian systems include time-reversal symmetry (TRS), particle-hole symmetry (PHS), chiral symmetry (CS), Hermitian conjugate symmetry of time-reversal symmetry (TRS^\dagger), Hermitian conjugate symmetry of particle-hole symmetry (PHS^\dagger), sublattice symmetry (SLS) and pseudo Hermitian symmetry[6]. The operators of these internal symmetries can be written in the general form,

$$\hat{O} = U_{\mathcal{O}} \hat{R}, \quad (1)$$

where $U_{\mathcal{O}}$ is a unitary matrix, \hat{R} the identity operator for unitary symmetries (PHS, PHS^\dagger , pseudo Hermitian symmetry) and the complex conjugate operator for anti-

unitary symmetries (TRS, TRS[†], CS, SLS). For a non-Hermitian Hamiltonian, $H(\mathbf{k})$, the transformation under an internal symmetry operation can be represented as

$$U_{\mathcal{O}}H(\mathbf{k})U_{\mathcal{O}}^{-1} = H^{\mathcal{O}}(\mathbf{k}), \quad (2)$$

where $U_{\mathcal{O}}$ is the unitary matrix given in Eq.(1). For general cases, the Hamiltonian $H(\mathbf{k})$ can be expressed in the general form

$$H(\mathbf{k}) = \sum_{\mathbf{j}} t_{\mathbf{j}} e^{i\mathbf{k}\cdot\mathbf{j}}, \quad (3)$$

where $\mathbf{j} = (j_1, j_2, \dots, j_d)$ denotes the hopping vector, $\mathbf{k} = (k_1, k_2, \dots, k_d)$ is the momentum vector in dD, and $t_{\mathbf{j}}$ is an $s \times s$ hopping matrix if the system which has s degrees of freedom (like orbital or sublattice) in a unit cell. When the system has an internal symmetry, the transformation of the matrix $t_{\mathbf{j}}$ under the corresponding internal symmetry is given by

$$U_{\mathcal{O}}t_{\mathbf{j}}U_{\mathcal{O}}^{-1} = t_{\mathbf{j}}^{\mathcal{O}}. \quad (4)$$

The forms of $H^{\mathcal{O}}(\mathbf{k})$ and $t_{\mathbf{j}}^{\mathcal{O}}$ for specific internal symmetries are given in Supplemental Materials[53].

Amoeba formulation— For 1D non-Hermitian systems, one can obtain the non-Bloch band theory by directly solving the lattice Schrödinger equation. However, for higher dimensional non-Hermitian systems, the boundary conditions of the Schrödinger equation on the lattice are much more complicated. As a consequence, the Schrödinger equation for higher dimensional non-Hermitian systems in general cannot be directly solved, and thereby a building of the the higher-dimensional non-Bloch band theory faces great challenging. Recently a remarkable progress in solving this fundamental problem is the recognition of the connection between the Amoeba formulation and the NHSE in arbitrary dimensions [50].

The Ronkin function is a key technique in the Amoeba formulation. For a non-Hermitian system, whose Hamiltonian under PBC is given by Eq.(3), the Ronkin function characterizing this system is of the form

$$R(E, H, \boldsymbol{\mu}) = \int_{T^d} \left(\frac{dk}{2\pi} \right)^d \ln \det [E - H(e^{\boldsymbol{\mu} + i\mathbf{k}})], \quad (5)$$

where $T^d = [0, 2\pi]^d$ denotes the dD torus, and

$$\begin{aligned} H(e^{\boldsymbol{\mu} + i\mathbf{k}}) &= H(e^{\mu_1 + ik_1}, \dots, e^{\mu_d + ik_d}) \\ &= \sum_{\mathbf{j}} t_{\mathbf{j}} e^{\mathbf{j}\cdot(\boldsymbol{\mu} + i\mathbf{k})} \end{aligned} \quad (6)$$

with $\boldsymbol{\mu}$ the vector reflecting the localization property of the skin modes. Consider a skin mode of the non-Hermitian system,

$$\psi_0(\mathbf{x}) = \beta_1^{x_1} \beta_2^{x_2} \dots \beta_d^{x_d} \psi, \quad (7)$$

\mathcal{O}	\mathcal{T}_+	\mathcal{C}_-	\mathcal{S}	\mathcal{C}_+	\mathcal{T}_-	Γ	η
$\tilde{E}_{\mathcal{O}}$	E^*	$-E$	$-E^*$	E	$-E^*$	$-E$	E^*
$\tilde{\boldsymbol{\mu}}_{\mathcal{O}}$	$\boldsymbol{\mu}$	$-\boldsymbol{\mu}$	$-\boldsymbol{\mu}$	$-\boldsymbol{\mu}$	$\boldsymbol{\mu}$	$\boldsymbol{\mu}$	$-\boldsymbol{\mu}$

TABLE I. The eigenenergy and decaying factor of the skin mode related to Eq.(12) for different internal symmetry. The first row is the internal symmetry, the second row is the value of $\tilde{E}_{\mathcal{O}}$, and the third row is the value of $\tilde{\boldsymbol{\mu}}_{\mathcal{O}}$ in Eq.(12) under the corresponding internal symmetry. \mathcal{T}_+ , \mathcal{C}_- , \mathcal{S} , \mathcal{C}_+ , \mathcal{T}_- , Γ and η represent TRS, PHS, CS, TRS[†], PHS[†], SLS and pseudo Hermitian symmetry, respectively.

where $\mathbf{x} = (x_1, x_2, \dots, x_d)$ is the position, $\beta_j = e^{\mu_{0,j} + ik_j}$ for the j th direction, and the eigenenergy of ψ_0 is denoted as E_0 [54]. According to the Amoeba formulation, the Ronkin function, $R(E_0, H, \boldsymbol{\mu})$, will take the minimum value if

$$\boldsymbol{\mu} = \boldsymbol{\mu}_0 = (\mu_{0,1}, \dots, \mu_{0,d}). \quad (8)$$

In other words, if E_0 belongs to the spectrum of the non-Hermitian system under OBC, and the eigenstate corresponding to it is ψ_0 given in Eq.(7), then the winding number

$$\begin{aligned} w_m &= \frac{1}{2\pi i} \int_0^{2\pi} dk_m \partial_{k_m} \ln \det [E - H(e^{\boldsymbol{\mu}_0 + i\mathbf{k}})] \\ &= 0 \quad \text{or} \quad \text{ill defined} \end{aligned} \quad (9)$$

for $\forall m = 1, 2, \dots, d$ [50][55](the derivation for Eq.(9) is given in Supplemental Materials[53]).

Constraints of internal symmetry on the NHSE— Now, we consider a non-Hermitian system, whose Hamiltonian under PBC is given by Eq.(3), and has an internal symmetry denoted by \mathcal{O} . Assume that this system has a skin mode with eigenenergy E and decaying factor

$$\boldsymbol{\mu} = (\mu_1, \dots, \mu_d). \quad (10)$$

We further define a winding number of the form

$$w_m^{\mathcal{O}} = \frac{1}{2\pi i} \int_0^{2\pi} dk_m \partial_{k_m} \ln \det [U_{\mathcal{O}} (E - H(e^{\boldsymbol{\mu} + i\mathbf{k}})) U_{\mathcal{O}}^{-1}]. \quad (11)$$

By a straightforward derivation (see more details in the Supplemental Materials[53]), we find that

$$w_m^{\mathcal{O}} = \pm \frac{1}{2\pi i} \int_0^{2\pi} dk_m \partial_{k_m} \ln \det [\tilde{E}_{\mathcal{O}} - H(e^{\tilde{\boldsymbol{\mu}}_{\mathcal{O}} + i\mathbf{k}})], \quad (12)$$

where $\tilde{E}_{\mathcal{O}} = \pm E$ or $\pm E^*$, and $\tilde{\boldsymbol{\mu}}_{\mathcal{O}} = \pm \boldsymbol{\mu}$ for different internal symmetries, as shown in Table I.

Next, using the fact that the determinant of a matrix does not change under a unitary transformation, i.e.,

$$\det [U_{\mathcal{O}} (E - H) U_{\mathcal{O}}^{-1}] = \det [(E - H)], \quad (13)$$

it is readily found that

$$w_m^{\mathcal{O}} = \frac{1}{2\pi i} \int_0^{2\pi} dk_m \partial_{k_m} \ln \det [E - H(e^{\mu+i\mathbf{k}})]. \quad (14)$$

As assumed in the beginning that this system has a skin mode with eigenenergy E and decaying factor μ , from the discussion around Eq.(7) we know that

$$w_m^{\mathcal{O}} = 0 \quad \text{or} \quad \text{ill defined}, \quad (15)$$

for $\forall m = 1, 2, \dots, d$. Applying this result back into Eq.(12), one can immediately reach the conclusion that if there exists a skin mode at E and a given boundary determined by the decaying factor μ , then there must exist another symmetry-enforced skin mode at $\tilde{E}_{\mathcal{O}}$ and the same place (for $\tilde{\mu}_{\mathcal{O}} = \mu$) or opposite boundaries (for $\tilde{\mu}_{\mathcal{O}} = -\mu$). The constraints of the seven internal symmetries on the NHSE summarized in Table I is one of the central results of this work.

Before proceeding, we would like to give a remark on the result shown in Table I. From the third column of Table I, one can see that the particle-hole symmetry enforces two particle-hole partner skin modes to localize at opposite boundaries. As aforementioned, this generic result has already been obtained in a previous work[36], however, the approach therein is much more involved and specific for the particle-hole symmetry. Thanks to the powerfulness of the Amoeba formulation for describing NHSE, here we have determined the complete picture in a rather neat way.

Example illustration.— To show the correctness of the analytical theory, we consider a 2D non-Hermitian system for illustration. The concrete Hamiltonian under PBC is given by

$$H_{\mathcal{T}_+}(k_x, k_y) = \begin{pmatrix} t_{-1}e^{-ik_x} + t_1e^{ik_x} & c + p_{-1}e^{-ik_y} \\ c + p_1e^{ik_y} & w_{-1}e^{-ik_x} + w_1e^{ik_x} \end{pmatrix}, \quad (16)$$

where $t_1, t_{-1}, p_1, p_{-1}, w_1, w_{-1}$ and c are real numbers. It is easy to check that the above Hamiltonian has TRS, and the TRS operator is given by

$$\hat{\mathcal{T}}_+ = \mathbf{I}_{2 \times 2} \mathcal{K}, \quad (17)$$

where $\mathbf{I}_{2 \times 2}$ is the 2×2 identity matrix and \mathcal{K} is the complex conjugate operator.

The spectra of this Hamiltonian under OBC for a specific set of parameter values are given in Fig.1(a). Consider two eigenstates related by TRS. Without loss of generality, we choose the pair with $E_{TRS1} = E_{TRS2}^* = -1.5 - 0.195i$ that are belonged to the OBC spectra. As shown in Figs.1(b) and 1(c), the probability density profile of these two skin modes are localized at the same boundary, agreeing with the prediction summarized in the second column of Table I. Examples for other internal symmetries are provided in the Supplemental

Materials[53], and all numerical results agree with the predictions summarized in Table I.

Bidirectional skin effect.— From Table I, one can see that the fifth column corresponding to TRS[†] is quite special since only for this symmetry $\tilde{E}_{\mathcal{O}} = E$. The invariance of E and the change of μ to $-\mu$ under the TRS[†] operation indicate that, under OBC, there will be two degenerate skin modes localizing at opposite boundaries of the system. However, we find that such degenerate skin modes are fragile. For general cases, the degeneracy disappears and the eigenstate is extended or simultaneously localized at two opposite boundaries. To illustrate this fact, we construct a simple 1D model of the form

$$H(k) = \begin{pmatrix} t_-e^{-ik} + t_+e^{ik} & \gamma \\ \gamma & t_-e^{ik} + t_+e^{-ik} \end{pmatrix}. \quad (18)$$

The TRS[†] operator for this system is

$$\hat{\mathcal{C}}_+ = U_{\mathcal{C}_+} \mathcal{K} = \begin{pmatrix} 0 & 1 \\ 1 & 0 \end{pmatrix} \mathcal{K}. \quad (19)$$

In the limit of $\gamma = 0$, the OBC spectra of this system are doubly degenerate, and two eigenstates corresponding to the same eigenenergy, E are localized at opposite boundaries (Fig.2). Once $\gamma \neq 0$, the double degeneracy of the OBC spectra is lifted, and we find eigenstates that are simultaneously localized at two opposite boundaries (Fig.3).

Remarkably, we find that the above phenomenon is in fact beyond the description of Amoeba formulation. To see this, let us return to the Amoeba formulation. Assuming that E belongs to the spectra of the system under OBC, the winding number about E for the Hamiltonian under PBC is

$$w_m^{PBC} = \frac{1}{2\pi i} \int_0^{2\pi} dk_m \partial_{k_m} \ln \det [E - H(\mathbf{k})], \quad (20)$$

where $m = 1, 2, \dots, d$. After the transformation of $U_{\mathcal{C}_+}$, we find that (see Supplemental Materials for details[53])

$$\begin{aligned} w_m^{PBC} &= \frac{1}{2\pi i} \int_0^{2\pi} dk_m \partial_{k_m} \ln \det [U_{\mathcal{C}_+} (E - H(\mathbf{k})) U_{\mathcal{C}_+}^{-1}] \\ &= \frac{1}{2\pi i} \int_0^{2\pi} dk_m \partial_{k_m} \ln \det [E - H(-\mathbf{k})^T] \\ &= -w_m^{PBC}. \end{aligned} \quad (21)$$

One immediately obtains

$$w_m^{PBC} = 0 \quad \text{or} \quad \text{ill defined}, \quad (22)$$

for $\forall m = 1, 2, \dots, d$. Since

$$H(\mathbf{k}) = H(e^{\mu+i\mathbf{k}})|_{\mu=0}, \quad (23)$$

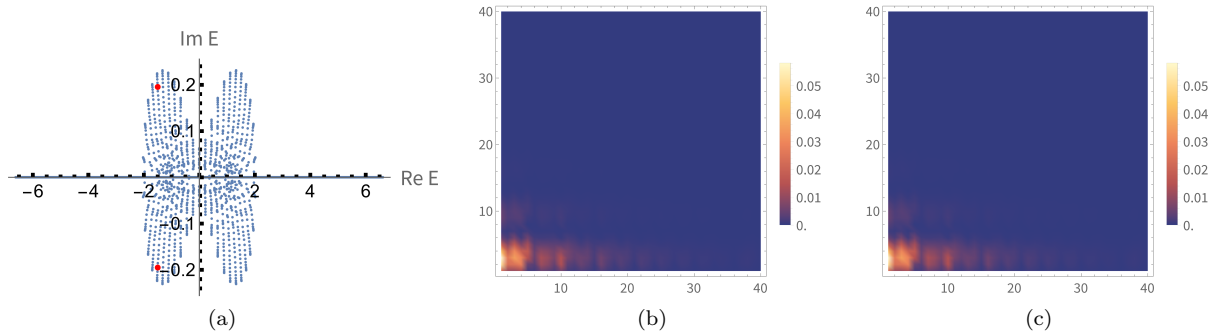


FIG. 1. (a)The blue dots refer to eigenenergies of the system given by Eq.(16) under OBC. The lower red dot corresponds to $E_{TRS1} = -1.5 - 0.195i$, and the upper one corresponds to $E_{TRS2} = -1.5 + 0.195i$. (b)The probability density profile corresponding to E_{TRS1} . (c)The probability density profile corresponding to E_{TRS2} . Values of parameters are $t_1 = 2$, $t_{-1} = 1$, $w_1 = 1.5$, $w_{-1} = 3.3$, $p_1 = 1.8$, $p_{-1} = 2.6$, and $c = 0.5$. The system size is 40×40 .

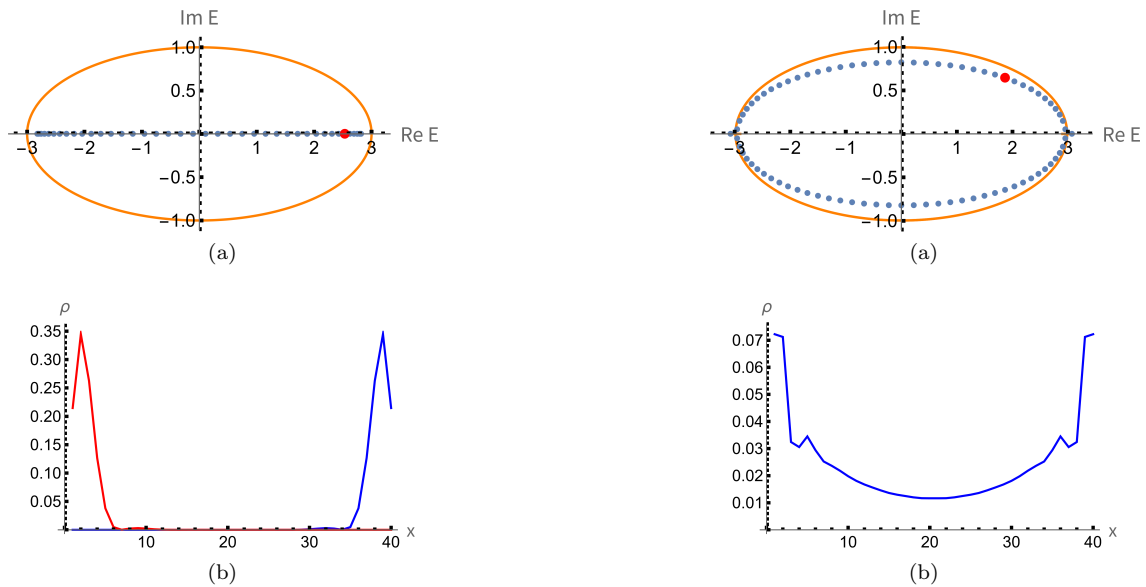


FIG. 2. (a)The blue dots refer to eigenenergies of the system given by Eq.(18) under OBC for the case that $\gamma = 0$, and the orange loop corresponds to the PBC spectrum for $\gamma = 0$. The two bands under PBC are degenerate, and both of them correspond to the same orange loop in the complex plane. The red dot corresponds to $E_{TRS\uparrow 1} = 2.53$. (b)The blue and red lines are the distributions of the two eigenstates corresponding to $E_{TRS\uparrow 1}$. Values of other parameters are $t_1 = 1$, $t_{-1} = 2$, and the system size is 40.

according to the Amoeba formulation, all eigenstates of this system are extended except for topological modes, which means that the NHSE does not exist in this system with TRS^\dagger . However, as shown above, we find that different from traditional skin modes, eigenstates can simultaneously localize at opposite boundaries. For the convenience of describing this phenomenon, we term it *bidirectional skin effect*. It may be worth emphasizing that here our findings can be applied to arbitrary dimen-

FIG. 3. (a)The blue dots are the locations of the eigenenergies of the system given by Eq.(18) under OBC for the case with $\gamma = 0.1$, and the orange loop corresponds to the PBC spectrum for $\gamma = 0.1$. The two bands under PBC are also degenerate, and both of them correspond to the same orange loop in the complex plane. The red dot is $E_{TRS\uparrow 2} = 1.87 + 0.64i$. (b)The blue line is the distribution of the eigenstate corresponding to $E_{TRS\uparrow 2}$. Values of other parameters are $t_1 = 1$, $t_{-1} = 2$, and the system size is 40.

sions. In 1D, the bidirectional skin effect is just reduced to the \mathbb{Z}_2 skin effect discovered in Ref.[41].

In the following, we develop a topological invariant to capture the bidirectional skin effect. The steps are as follows. First, we note that the winding number in Eq.(20)

can be rewritten as

$$\begin{aligned} w_m^{PBC}(E) &= \frac{1}{2\pi i} \int_0^{2\pi} dk_m \partial_{k_m} \ln \left[\prod_{n=1}^{2N} E - E_n(\mathbf{k}) \right] \\ &= \sum_{n=1}^{2N} \frac{1}{2\pi i} \int_0^{2\pi} dk_m \partial_{k_m} \ln [E - E_n(\mathbf{k})] \quad (24) \\ &= \sum_{n=1}^{2N} w_m^{(n)}(E), \end{aligned}$$

where $E_n(\mathbf{k})$ is the n th band of the system under PBC, and

$$w_m^{(n)}(E) = \frac{1}{2\pi i} \int_0^{2\pi} dk_m \partial_{k_m} \ln [E - E_n(\mathbf{k})], \quad (25)$$

is the winding number of the n th band. We find that if under OBC the eigenstate at E is extended, then

$$w_m^{(n)}(E) = 0 \quad (26)$$

for $\forall m = 1, 2, \dots, d$, and $n = 1, 2, \dots, 2N$. In contrast, if the eigenstate is simultaneously localized at opposite boundaries, pairs of non-zero winding numbers will appear[56], i.e.,

$$w_m^{(p)}(E) = -w_m^{(q)}(E) \neq 0, \quad (27)$$

where the q th band is related to the p th band by TRS^\dagger , i.e.,

$$E_q(\mathbf{k}) = \hat{C}_+ E_p(\mathbf{k}). \quad (28)$$

Therefore, for a non-Hermitian system with TRS^\dagger , whether the eigenstate at a given E is a bidirectional skin mode or not can be described by

$$\nu_m(E) = \frac{1}{2} \sum_{n=0}^{N-1} |w_m^{(2n+1)}(E) - w_m^{(2n+2)}(E)|, \quad (29)$$

where $m = 1, 2, \dots, d$. Here the $(2n+1)$ th and $(2n+2)$ th bands are related by TRS^\dagger , and the system has $2N$ bands in total [57]. We call these topological invariants TRS^\dagger winding numbers. If $\nu_m(E) = 0$ for $\forall m = 1, 2, \dots, d$, the eigenstate at E is extended in the bulk. In contrast, if $\nu_m(E) \neq 0$ for one or more $\nu_m(E)$, the eigenstate at E is a bidirectional skin mode. See the spectrum shown in Fig.3(a), it is not hard to find that for the bidirectional skin mode corresponding to $E_{\text{TRS}^\dagger 2}$, $\nu(E_{\text{TRS}^\dagger 2}) = 1$ [58]. Examples for bidirectional skin effect in 2D non-Hermitian systems are given in Supplemental Materials[53].

Conclusion and discussion— In this Letter, we have systematically investigated the behavior of NHSE under various internal symmetries based on the Amoeba formulation and obtained their constraints on the NHSE.

We find that for a non-Hermitian system with an internal symmetry \mathcal{O} , if it has a skin mode with a decaying factor $\boldsymbol{\mu}$ and at eigenenergy E , then there must exist another skin mode at eigenenergy $\tilde{E}_{\mathcal{O}}$, which localizes at the same (opposite) boundary of the original skin mode if $\tilde{\boldsymbol{\mu}}_{\mathcal{O}} = \boldsymbol{\mu}$ ($\tilde{\boldsymbol{\mu}}_{\mathcal{O}} = -\boldsymbol{\mu}$). Furthermore, we have found the bidirectional skin effect in non-Hermitian systems with TRS^\dagger , and we have introduced a topological invariant named as TRS^\dagger winding numbers to describe this phenomenon. From the aspect of 38-fold symmetry classes, for a non-Hermitian system with symmetry class \mathcal{Q} , if \mathcal{Q} contains TRS^\dagger , the system can have bidirectional skin effect, otherwise, only the conventional skin effect is allowed. To conclude, we have established the overall picture of the relation between the internal symmetry and the NHSE. As our findings neither rely on the dimension nor specific non-Hermitian Hamiltonians, they admit a wide application. In experiment, the ultracold-atom systems can be utilized as the platform to observe the novel behaviors of non-Hermitian skin effect under internal symmetries[35, 36, 59]. Furthermore, our formula can be used to research the properties of non-Hermitian skin effect under crystalline symmetries and this is a focus in our future work.

Acknowledgements— The author thanks Zhongbo Yan for helpful suggestions. This work is supported by the National Natural Science Foundation of China (Grant No.12174455) and the Natural Science Foundation of Guangdong Province (Grant No.2021B1515020026).

* wangshx65@mail.sysu.edu.cn

- [1] I. Rotter, A non-hermitian hamilton operator and the physics of open quantum systems, *Journal of Physics A: Mathematical and Theoretical* **42**, 153001 (2009).
- [2] H. J. Carmichael, Quantum trajectory theory for cascaded open systems, *Phys. Rev. Lett.* **70**, 2273 (1993).
- [3] S. Malzard, C. Poli, and H. Schomerus, Topologically protected defect states in open photonic systems with non-hermitian charge-conjugation and parity-time symmetry, *Phys. Rev. Lett.* **115**, 200402 (2015).
- [4] A. McDonald, R. Hanai, and A. A. Clerk, Nonequilibrium stationary states of quantum non-hermitian lattice models, *Phys. Rev. B* **105**, 064302 (2022).
- [5] H. Shen, B. Zhen, and L. Fu, Topological band theory for non-hermitian hamiltonians, *Phys. Rev. Lett.* **120**, 146402 (2018).
- [6] K. Kawabata, K. Shiozaki, M. Ueda, and M. Sato, Symmetry and topology in non-hermitian physics, *Phys. Rev. X* **9**, 041015 (2019).
- [7] T. E. Lee, Anomalous edge state in a non-hermitian lattice, *Phys. Rev. Lett.* **116**, 133903 (2016).
- [8] S. Yao and Z. Wang, Edge states and topological invariants of non-hermitian systems, *Phys. Rev. Lett.* **121**, 086803 (2018).
- [9] S. Yao, F. Song, and Z. Wang, Non-hermitian chern bands, *Phys. Rev. Lett.* **121**, 136802 (2018).

- [10] K. Yokomizo and S. Murakami, Non-bloch band theory of non-hermitian systems, *Phys. Rev. Lett.* **123**, 066404 (2019).
- [11] K. Kawabata, N. Okuma, and M. Sato, Non-bloch band theory of non-hermitian hamiltonians in the symplectic class, *Phys. Rev. B* **101**, 195147 (2020).
- [12] W.-T. Xue, M.-R. Li, Y.-M. Hu, F. Song, and Z. Wang, Simple formulas of directional amplification from non-bloch band theory, *Phys. Rev. B* **103**, L241408 (2021).
- [13] H. Li and S. Wan, Exact formulas of the end-to-end green's functions in non-hermitian systems, *Phys. Rev. B* **105**, 045122 (2022).
- [14] K. Kawabata, K. Shiozaki, and S. Ryu, Topological field theory of non-hermitian systems, *Phys. Rev. Lett.* **126**, 216405 (2021).
- [15] Z. Yang, K. Zhang, C. Fang, and J. Hu, Non-hermitian bulk-boundary correspondence and auxiliary generalized brillouin zone theory, *Phys. Rev. Lett.* **125**, 226402 (2020).
- [16] M. M. Denner, A. Skurativska, F. Schindler, M. H. Fischer, R. Thomale, T. Bzdušek, and T. Neupert, Exceptional topological insulators, *Nature communications* **12**, 5681 (2021).
- [17] Y. Fu and S. Wan, Degeneracy and defectiveness in non-hermitian systems with open boundary, *Phys. Rev. B* **105**, 075420 (2022).
- [18] Z. Yang, A. P. Schnyder, J. Hu, and C.-K. Chiu, Fermion doubling theorems in two-dimensional non-hermitian systems for fermi points and exceptional points, *Phys. Rev. Lett.* **126**, 086401 (2021).
- [19] H. Hu and E. Zhao, Knots and non-hermitian bloch bands, *Phys. Rev. Lett.* **126**, 010401 (2021).
- [20] K. Kawabata, T. Bessho, and M. Sato, Classification of exceptional points and non-hermitian topological semimetals, *Phys. Rev. Lett.* **123**, 066405 (2019).
- [21] M. Stålhammar and E. J. Bergholtz, Classification of exceptional nodal topologies protected by \mathcal{PT} symmetry, *Phys. Rev. B* **104**, L201104 (2021).
- [22] W. Tang, X. Jiang, K. Ding, Y.-X. Xiao, Z.-Q. Zhang, C. T. Chan, and G. Ma, Exceptional nexus with a hybrid topological invariant, *Science* **370**, 1077 (2020), <https://www.science.org/doi/pdf/10.1126/science.abd8872>.
- [23] H. Hu, S. Sun, and S. Chen, Knot topology of exceptional point and non-hermitian no-go theorem, *Phys. Rev. Res.* **4**, L022064 (2022).
- [24] I. Mandal and E. J. Bergholtz, Symmetry and higher-order exceptional points, *Phys. Rev. Lett.* **127**, 186601 (2021).
- [25] K. Yokomizo and S. Murakami, Topological semimetal phase with exceptional points in one-dimensional non-hermitian systems, *Phys. Rev. Res.* **2**, 043045 (2020).
- [26] T. Liu, J. J. He, Z. Yang, and F. Nori, Higher-order weyl-exceptional-ring semimetals, *Phys. Rev. Lett.* **127**, 196801 (2021).
- [27] F. Song, H.-Y. Wang, and Z. Wang, Non-bloch PT symmetry: Universal threshold and dimensional surprise, in *A Festschrift in Honor of the C N Yang Centenary* (WORLD SCIENTIFIC, 2022) pp. 299–311.
- [28] Y.-M. Hu, H.-Y. Wang, Z. Wang, and F. Song, Geometric origin of non-bloch pt symmetry breaking (2022), [arXiv:2210.13491](https://arxiv.org/abs/2210.13491) [quant-ph].
- [29] W.-T. Xue, Y.-M. Hu, F. Song, and Z. Wang, Non-hermitian edge burst, *Phys. Rev. Lett.* **128**, 120401 (2022).
- [30] L. Xiao, W.-T. Xue, F. Song, Y.-M. Hu, W. Yi, Z. Wang, and P. Xue, Observation of non-hermitian edge burst in quantum dynamics (2023), [arXiv:2303.12831](https://arxiv.org/abs/2303.12831) [cond-mat.mes-hall].
- [31] P. Wen, J. Pi, and G. Long, Real space analysis for edge burst in a non-hermitian quantum walk model (2023), [arXiv:2303.17219](https://arxiv.org/abs/2303.17219) [quant-ph].
- [32] Y.-M. Hu, W.-T. Xue, F. Song, and Z. Wang, Many-body edge burst in steady states (2023), [arXiv:2306.08676](https://arxiv.org/abs/2306.08676) [quant-ph].
- [33] T. Ozawa, H. M. Price, A. Amo, N. Goldman, M. Hafezi, L. Lu, M. C. Rechtsman, D. Schuster, J. Simon, O. Zeitlinger, and I. Carusotto, Topological photonics, *Rev. Mod. Phys.* **91**, 015006 (2019).
- [34] H. Zhao, X. Qiao, T. Wu, B. Midya, S. Longhi, and L. Feng, Non-hermitian topological light steering, *Science* **365**, 1163 (2019), <https://www.science.org/doi/pdf/10.1126/science.aay1064>.
- [35] Q. Liang, D. Xie, Z. Dong, H. Li, H. Li, B. Gadway, W. Yi, and B. Yan, Dynamic signatures of non-hermitian skin effect and topology in ultracold atoms, *Phys. Rev. Lett.* **129**, 070401 (2022).
- [36] Z.-Y. Wang, J.-S. Hong, and X.-J. Liu, Symmetric non-hermitian skin effect with emergent nonlocal correspondence, *Phys. Rev. B* **108**, L060204 (2023).
- [37] K. Ding, G. Ma, Z. Q. Zhang, and C. T. Chan, Experimental demonstration of an anisotropic exceptional point, *Phys. Rev. Lett.* **121**, 085702 (2018).
- [38] Q. Zhang, Y. Li, H. Sun, X. Liu, L. Zhao, X. Feng, X. Fan, and C. Qiu, Observation of acoustic non-hermitian bloch braids and associated topological phase transitions, *Phys. Rev. Lett.* **130**, 017201 (2023).
- [39] C. H. Lee and R. Thomale, Anatomy of skin modes and topology in non-hermitian systems, *Phys. Rev. B* **99**, 201103 (2019).
- [40] K. Zhang, Z. Yang, and C. Fang, Correspondence between winding numbers and skin modes in non-hermitian systems, *Phys. Rev. Lett.* **125**, 126402 (2020).
- [41] N. Okuma, K. Kawabata, K. Shiozaki, and M. Sato, Topological origin of non-hermitian skin effects, *Phys. Rev. Lett.* **124**, 086801 (2020).
- [42] H. Li and S. Wan, Dynamic skin effects in non-hermitian systems, *Phys. Rev. B* **106**, L241112 (2022).
- [43] K. Zhang, Z. Yang, and C. Fang, Universal non-hermitian skin effect in two and higher dimensions, *Nature communications* **13**, 2496 (2022).
- [44] L. Li, C. H. Lee, and J. Gong, Impurity induced scale-free localization, *Communications Physics* **4**, 42 (2021).
- [45] P. Mognini, O. Arandes, and E. J. Bergholtz, Anomalous skin effects in disordered systems with a single non-hermitian impurity, *Phys. Rev. Res.* **5**, 033058 (2023).
- [46] J. Sun, C.-A. Li, S. Feng, and H. Guo, Hybrid higher-order skin-topological effect in hyperbolic lattices, *Phys. Rev. B* **108**, 075122 (2023).
- [47] Y. Fu and Y. Zhang, Hybrid skin-scale-free effect in non-hermitian systems: A transfer matrix approach (2023), [arXiv:2307.16632](https://arxiv.org/abs/2307.16632) [cond-mat.mes-hall].
- [48] M. Lu, X.-X. Zhang, and M. Franz, Magnetic suppression of non-hermitian skin effects, *Phys. Rev. Lett.* **127**, 256402 (2021).
- [49] C.-A. Li, B. Trauzettel, T. Neupert, and S.-B. Zhang, Enhancement of second-order non-hermitian skin effect by magnetic fields, *Phys. Rev. Lett.* **131**, 116601 (2023).
- [50] H.-Y. Wang, F. Song, and Z. Wang, Amoeba formula-

- tion of the non-hermitian skin effect in higher dimensions (2022), arXiv:2212.11743 [cond-mat.mes-hall].
- [51] H. Hu, Non-hermitian band theory in all dimensions: uniform spectra and skin effect (2023), arXiv:2306.12022 [cond-mat.mes-hall].
- [52] A. Banerjee, R. Jaiswal, M. Manjunath, and A. Narayan, A tropical geometric approach to exceptional points, Proceedings of the National Academy of Sciences **120**, e2302572120 (2023), <https://www.pnas.org/doi/pdf/10.1073/pnas.2302572120>.
- [53] See supplemental materials at for details., .
- [54] Due to OBC, the wave function corresponding to E_0 is a linear combination of many modes. However, contributions of some modes vanish in the thermodynamic limit. The rest of the modes have the same vector $\boldsymbol{\mu}$. That means the localization property of these modes are the same. This work only concerns the localization property of the wave function, thus the wave function can be written as the form in Eq.(7) .
- [55] According to Ref.[50], the Ronkin function is convex in the entire $\boldsymbol{\mu}$ space, thus Eq.(9) is the condition for the minimum value of Ronkin function. The Amoeba formulation also point out that if E belongs to the OBC spectrum of the non-Hermitian system and the wave function corresponding to E has the decaying factor, $\boldsymbol{\mu}_0$, then there existss a vector, \mathbf{k}_0 , such that E is an eigenvalue of $H(e^{\boldsymbol{\mu}_0 + i\mathbf{k}_0})$. Thus for specific value of \mathbf{k} , the winding number in Eq.(9) is ill defined.
- [56] For general cases, the band, $E_\mu(\mathbf{k})$, is multi-valued. Here, we always choose the branch that makes $E_\mu(\mathbf{k})$ be a closed loop but not an open curve in the complex plane.
- [57] If the number of bands is odd, there exists a band, $E_r(\mathbf{k})$, such that $E_r(\mathbf{k}) = \hat{C}_+ E_r(\mathbf{k})$. The winding number of this band, $w_m^{(r)}(E)$ must be zero and gives no contribution to the topological invariant, $\nu_m(E)$. Hence, we only consider the case that the system has an even number of bands.
- [58] For the case that $\gamma = 0$ shown in Fig.2, it is also not hard to find that $\nu(E_{TRS\pm 1}) = 1$. On the other hand, two degenerate skin modes corresponding to $E_{TRS\pm 1}$ can consist of two states, which are localized at opposite boundaries. Thus, this case can be seen as a special case of bidirectional skin effect.
- [59] Z. Ren, D. Liu, E. Zhao, C. He, K. K. Pak, J. Li, and G.-B. Jo, Chiral control of quantum states in non-hermitian spin-orbit-coupled fermions, Nature Physics **18**, 385 (2022).

Supplemental Material

TRANSFORMATION OF HAMILTONIAN UNDER INTERNAL SYMMETRIES

In this section, we give the specific form of $H^{\mathcal{O}}(\mathbf{k})$ and $t_j^{\mathcal{O}}$ in Eq.(2) and Eq.(4) in main text.

According to Ref.[6], for the non-Hermitian Hamiltonian, $H(\mathbf{k})$, the transformation of it under internal symmetries can be represented as

$$U_{\mathcal{T}_+} H(\mathbf{k}) U_{\mathcal{T}_+}^{-1} = H^*(-\mathbf{k}), \quad (\text{S1})$$

$$U_{\mathcal{C}_-} H(\mathbf{k}) U_{\mathcal{C}_-}^{-1} = -H^T(-\mathbf{k}), \quad (\text{S2})$$

$$U_{\mathcal{S}} H(\mathbf{k}) U_{\mathcal{S}}^{-1} = -H^\dagger(\mathbf{k}), \quad (\text{S3})$$

$$U_{\mathcal{C}_+} H(\mathbf{k}) U_{\mathcal{C}_+}^{-1} = H^T(-\mathbf{k}), \quad (\text{S4})$$

$$U_{\mathcal{T}_-} H(\mathbf{k}) U_{\mathcal{T}_-}^{-1} = -H^*(-\mathbf{k}), \quad (\text{S5})$$

$$U_{\Gamma} H(\mathbf{k}) U_{\Gamma}^{-1} = -H(\mathbf{k}), \quad (\text{S6})$$

$$U_{\eta} H(\mathbf{k}) U_{\eta}^{-1} = H^\dagger(\mathbf{k}), \quad (\text{S7})$$

where $U_{\mathcal{T}_+}$, $U_{\mathcal{C}_-}$, $U_{\mathcal{S}}$, $U_{\mathcal{C}_+}$, $U_{\mathcal{T}_-}$, U_{Γ} and U_{η} are unitary matrix of TRS, PHS, CS, TRS[†], PHS[†], SLS and pseudo Hermitian symmetry respectively. Substituting $H(\mathbf{k})$ in Eq.(3) into equations above, we obtain the the transformation of matrix t_j under the internal symmetries,

$$U_{\mathcal{T}_+} t_j U_{\mathcal{T}_+}^{-1} = t_j^*, \quad (\text{S8})$$

$$U_{\mathcal{C}_-} t_j U_{\mathcal{C}_-}^{-1} = -t_{-j}^T, \quad (\text{S9})$$

$$U_{\mathcal{S}} t_j U_{\mathcal{S}}^{-1} = -t_{-j}^\dagger, \quad (\text{S10})$$

$$U_{\mathcal{C}_+} t_j U_{\mathcal{C}_+}^{-1} = t_{-j}^T, \quad (\text{S11})$$

$$U_{\mathcal{T}_-} t_j U_{\mathcal{T}_-}^{-1} = -t_j^*, \quad (\text{S12})$$

$$U_{\Gamma} t_j U_{\Gamma}^{-1} = -t_j, \quad (\text{S13})$$

$$U_{\eta} t_j U_{\eta}^{-1} = t_{-j}^\dagger. \quad (\text{S14})$$

DERVIATION FOR EQ.(9)

The Ronkin function about the non-Hermitian system is

$$R(E, H, \boldsymbol{\mu}) = \int_{T^d} \left(\frac{dk}{2\pi} \right)^d \ln \det [E - H(e^{\boldsymbol{\mu} + i\mathbf{k}})] \quad (\text{S15})$$

If $R(E, H, \boldsymbol{\mu})$ takes the minimum value at

$$\boldsymbol{\mu} = \boldsymbol{\mu}_0 = (\mu_{0,1}, \dots, \mu_{0,d}), \quad (\text{S16})$$

$R(E, H, \boldsymbol{\mu})$ satisfies

$$\left. \frac{\partial R(E, H, \boldsymbol{\mu})}{\partial \mu_j} \right|_{\boldsymbol{\mu}=\boldsymbol{\mu}_0} = \int_{T^d} \left(\frac{dk}{2\pi} \right)^d \left. \frac{\partial}{\partial \mu_j} \ln \det [E - H(e^{\boldsymbol{\mu} + i\mathbf{k}})] \right|_{\boldsymbol{\mu}=\boldsymbol{\mu}_0} = 0 \quad (\text{S17})$$

for $j = 1, 2, \dots, d$. Since

$$H(e^{\boldsymbol{\mu} + i\mathbf{k}}) = H(e^{\mu_1 + ik_1}, \dots, e^{\mu_d + ik_d}), \quad (\text{S18})$$

we can replace $\frac{\partial}{\partial \mu_i}$ with $-i \frac{\partial}{\partial k_j}$ in Eq.(S17). After that, Eq.(S17) can be written as

$$\left. \frac{\partial R(E, H, \boldsymbol{\mu})}{\partial \mu_j} \right|_{\boldsymbol{\mu}=\boldsymbol{\mu}_0} = -i \int_{T^d} \left(\frac{dk}{2\pi} \right)^d \frac{\partial}{\partial k_j} \ln \det [E - H(e^{\boldsymbol{\mu}_0 + i\mathbf{k}})] = 0. \quad (\text{S19})$$

The value of the winding number

$$w_j = \frac{1}{2\pi i} \int_0^{2\pi} dk_j \frac{\partial}{\partial k_j} \ln \det [E - H(e^{\mu_0 + i\mathbf{k}})] \quad (\text{S20})$$

is a constant. Hence,

$$-i \int_{T^d} \left(\frac{dk}{2\pi} \right)^d \frac{\partial}{\partial k_j} \ln \det [E - H(e^{\mu_0 + i\mathbf{k}})] = \int_{T^{d-1}} \left(\frac{dk}{2\pi} \right)^{d-1} w_j = w_j. \quad (\text{S21})$$

Thus, the condition for the minimum value of Ronkin function is

$$w_j = 0 \quad \text{or} \quad \text{ill defined} \quad (\text{S22})$$

for $\forall m = 1, 2, \dots, d$, i.e. Eq.(9) in the main text.

RESULTS IN EQ.(12) AND TABLE I

In this section, we give the demonstrations about results given in Eq.(12) and table **I** in the main text.

Properties about the expression of winding number

Consider a $s \times s$ matrix, $A(k)$, which depend on the parameter, k . Then, the winding number of A about E is

$$w(E) = \frac{1}{2\pi i} \int_0^{2\pi} dk \partial_k \ln \det [E - A(k)]. \quad (\text{S23})$$

There are 4 useful properties about the winding number for the following demonstrations,

$$\begin{aligned} w_{A1}(E) &= \frac{1}{2\pi i} \int_0^{2\pi} dk \partial_k \ln \det [E - A(-k)] \\ &= \frac{1}{2\pi i} \int_{2\pi}^0 d(-k) \partial_{-k} \ln \det [E - A(-k)] \\ &= \frac{-1}{2\pi i} \int_0^{2\pi} dk \partial_k \ln \det [E - A(k)] \\ &= -w(E), \end{aligned} \quad (\text{S24})$$

$$\begin{aligned} w_{A2}(E) &= \frac{1}{2\pi i} \int_0^{2\pi} dk \partial_k \ln \det [E - A^T(k)] \\ &= \frac{1}{2\pi i} \int_0^{2\pi} dk \partial_k \ln \det [(E - A(k))^T] \\ &= \frac{1}{2\pi i} \int_0^{2\pi} dk \partial_k \ln \det [E - A(k)] \\ &= w(E), \end{aligned} \quad (\text{S25})$$

$$\begin{aligned} w_{A3}(E) &= \frac{1}{2\pi i} \int_0^{2\pi} dk \partial_k \ln \det [E + A(k)] \\ &= \frac{1}{2\pi i} \int_0^{2\pi} dk \partial_k \ln \{(-1)^s \det [-E - A(k)]\} \\ &= \frac{1}{2\pi i} \int_0^{2\pi} dk \partial_k \ln \det [-E - A(k)], \end{aligned} \quad (\text{S26})$$

$$\begin{aligned}
w_{A_4}(E) &= \frac{1}{2\pi i} \int_0^{2\pi} dk \partial_k \ln \det [E - A^*(k)] \\
&= \left(\frac{-1}{2\pi i} \int_0^{2\pi} dk \partial_k \ln \det [E^* - A(k)] \right)^* \\
&= \frac{-1}{2\pi i} \int_0^{2\pi} dk \partial_k \ln \det [E^* - A(k)].
\end{aligned} \tag{S27}$$

TRS

According to Eq.(11) in the main text,

$$w_m^{\mathcal{T}_+}(E) = \frac{1}{2\pi i} \int_0^{2\pi} dk_m \partial_{k_m} \ln \det \left[U_{\mathcal{T}_+} (E - H(e^{\boldsymbol{\mu} + i\mathbf{k}})) U_{\mathcal{T}_+}^{-1} \right]. \tag{S28}$$

$H(e^{\boldsymbol{\mu} + i\mathbf{k}})$ is given in Eq.(18). Thus,

$$w_m^{\mathcal{T}_+}(E) = \frac{1}{2\pi i} \int_0^{2\pi} dk_m \partial_{k_m} \ln \det \left[E - \sum_{\mathbf{j}} U_{\mathcal{T}_+} t_{\mathbf{j}} U_{\mathcal{T}_+}^{-1} e^{\mathbf{j} \cdot (\boldsymbol{\mu} + i\mathbf{k})} \right]. \tag{S29}$$

Substituting Eq.(S8) into Eq.(S29), we get

$$\begin{aligned}
w_m^{\mathcal{T}_+}(E) &= \frac{1}{2\pi i} \int_0^{2\pi} dk_m \partial_{k_m} \ln \det \left[E - \sum_{\mathbf{j}} t_{\mathbf{j}}^* e^{\mathbf{j} \cdot (\boldsymbol{\mu} + i\mathbf{k})} \right] \\
&= \frac{1}{2\pi i} \int_0^{2\pi} dk_m \partial_{k_m} \ln \det \left[E - \sum_{\mathbf{j}} \left(t_{\mathbf{j}} e^{\mathbf{j} \cdot (\boldsymbol{\mu} - i\mathbf{k})} \right)^* \right] \\
&= \frac{-1}{2\pi i} \int_0^{2\pi} dk_m \partial_{k_m} \ln \det \left[E^* - \sum_{\mathbf{j}} t_{\mathbf{j}} e^{\mathbf{j} \cdot (\boldsymbol{\mu} - i\mathbf{k})} \right] \\
&= \frac{1}{2\pi i} \int_0^{2\pi} dk_m \partial_{k_m} \ln \det \left[E^* - \sum_{\mathbf{j}} t_{\mathbf{j}} e^{\mathbf{j} \cdot (\boldsymbol{\mu} + i\mathbf{k})} \right] \\
&= \frac{1}{2\pi i} \int_0^{2\pi} dk_m \partial_{k_m} \ln \det [E^* - H(e^{\boldsymbol{\mu} + i\mathbf{k}})].
\end{aligned} \tag{S30}$$

Thus, $\tilde{E}_{\mathcal{T}_+} = E^*$, $\tilde{\boldsymbol{\mu}}_{\mathcal{T}_+} = \boldsymbol{\mu}$.

PHS

$$\begin{aligned}
w_m^{\mathcal{C}_-}(E) &= \frac{1}{2\pi i} \int_0^{2\pi} dk_m \partial_{k_m} \ln \det \left[E - \sum_{\mathbf{j}} U_{\mathcal{C}_-} t_{\mathbf{j}} U_{\mathcal{C}_-}^{-1} e^{\mathbf{j} \cdot (\boldsymbol{\mu} + i\mathbf{k})} \right] \\
&= \frac{1}{2\pi i} \int_0^{2\pi} dk_m \partial_{k_m} \ln \det \left[E + \sum_{\mathbf{j}} t_{-\mathbf{j}}^T e^{\mathbf{j} \cdot (\boldsymbol{\mu} + i\mathbf{k})} \right] \\
&= \frac{1}{2\pi i} \int_0^{2\pi} dk_m \partial_{k_m} \ln \det \left[E + \sum_{\mathbf{j}} t_{\mathbf{j}} e^{\mathbf{j} \cdot (-\boldsymbol{\mu} - i\mathbf{k})} \right] \\
&= \frac{1}{2\pi i} \int_0^{2\pi} dk_m \partial_{k_m} \ln \det \left[-E - \sum_{\mathbf{j}} t_{\mathbf{j}} e^{\mathbf{j} \cdot (-\boldsymbol{\mu} - i\mathbf{k})} \right] \\
&= \frac{-1}{2\pi i} \int_0^{2\pi} dk_m \partial_{k_m} \ln \det \left[-E - \sum_{\mathbf{j}} t_{\mathbf{j}} e^{\mathbf{j} \cdot (-\boldsymbol{\mu} + i\mathbf{k})} \right] \\
&= \frac{-1}{2\pi i} \int_0^{2\pi} dk_m \partial_{k_m} \ln \det \left[-E - H(e^{-\boldsymbol{\mu} + i\mathbf{k}}) \right].
\end{aligned} \tag{S31}$$

Thus, $\tilde{E}_{\mathcal{C}_-} = -E$, $\tilde{\boldsymbol{\mu}}_{\mathcal{C}_-} = -\boldsymbol{\mu}$.

CS

$$\begin{aligned}
w_m^{\mathcal{S}}(E) &= \frac{1}{2\pi i} \int_0^{2\pi} dk_m \partial_{k_m} \ln \det \left[E - \sum_{\mathbf{j}} U_{\mathcal{S}} t_{\mathbf{j}} U_{\mathcal{S}}^{-1} e^{\mathbf{j} \cdot (\boldsymbol{\mu} + i\mathbf{k})} \right] \\
&= \frac{1}{2\pi i} \int_0^{2\pi} dk_m \partial_{k_m} \ln \det \left[E + \sum_{\mathbf{j}} t_{-\mathbf{j}}^\dagger e^{\mathbf{j} \cdot (\boldsymbol{\mu} + i\mathbf{k})} \right] \\
&= \frac{1}{2\pi i} \int_0^{2\pi} dk_m \partial_{k_m} \ln \det \left[-E - \sum_{\mathbf{j}} t_{-\mathbf{j}}^* e^{\mathbf{j} \cdot (\boldsymbol{\mu} + i\mathbf{k})} \right] \\
&= \frac{1}{2\pi i} \int_0^{2\pi} dk_m \partial_{k_m} \ln \det \left[-E - \sum_{\mathbf{j}} \left(t_{\mathbf{j}} e^{\mathbf{j} \cdot (-\boldsymbol{\mu} + i\mathbf{k})} \right)^* \right] \\
&= \frac{-1}{2\pi i} \int_0^{2\pi} dk_m \partial_{k_m} \ln \det \left[-E^* - \sum_{\mathbf{j}} t_{\mathbf{j}} e^{\mathbf{j} \cdot (-\boldsymbol{\mu} + i\mathbf{k})} \right] \\
&= \frac{-1}{2\pi i} \int_0^{2\pi} dk_m \partial_{k_m} \ln \det \left[-E^* - H(e^{-\boldsymbol{\mu} + i\mathbf{k}}) \right].
\end{aligned} \tag{S32}$$

Thus, $\tilde{E}_{\mathcal{S}} = -E^*$, $\tilde{\boldsymbol{\mu}}_{\mathcal{S}} = -\boldsymbol{\mu}$.

TRS[†]

$$\begin{aligned}
w_m^{C_+}(E) &= \frac{1}{2\pi i} \int_0^{2\pi} dk_m \partial_{k_m} \ln \det \left[E - \sum_{\mathbf{j}} U_{C_+} t_{\mathbf{j}} U_{C_+}^{-1} e^{\mathbf{j} \cdot (\boldsymbol{\mu} + i\mathbf{k})} \right] \\
&= \frac{1}{2\pi i} \int_0^{2\pi} dk_m \partial_{k_m} \ln \det \left[E - \sum_{\mathbf{j}} t_{-\mathbf{j}}^T e^{\mathbf{j} \cdot (\boldsymbol{\mu} + i\mathbf{k})} \right] \\
&= \frac{1}{2\pi i} \int_0^{2\pi} dk_m \partial_{k_m} \ln \det \left[E - \sum_{\mathbf{j}} t_{\mathbf{j}} e^{\mathbf{j} \cdot (-\boldsymbol{\mu} - i\mathbf{k})} \right] \\
&= \frac{-1}{2\pi i} \int_0^{2\pi} dk_m \partial_{k_m} \ln \det \left[E - \sum_{\mathbf{j}} t_{\mathbf{j}} e^{\mathbf{j} \cdot (-\boldsymbol{\mu} + i\mathbf{k})} \right] \\
&= \frac{-1}{2\pi i} \int_0^{2\pi} dk_m \partial_{k_m} \ln \det [E - H(e^{-\boldsymbol{\mu} + i\mathbf{k}})]
\end{aligned} \tag{S33}$$

Thus, $\tilde{E}_{C_+} = E$, $\tilde{\boldsymbol{\mu}}_{C_+} = -\boldsymbol{\mu}$.

PHS[†]

$$\begin{aligned}
w_m^{\mathcal{T}_-}(E) &= \frac{1}{2\pi i} \int_0^{2\pi} dk_m \partial_{k_m} \ln \det \left[E - \sum_{\mathbf{j}} U_{\mathcal{T}_-} t_{\mathbf{j}} U_{\mathcal{T}_-}^{-1} e^{\mathbf{j} \cdot (\boldsymbol{\mu} + i\mathbf{k})} \right] \\
&= \frac{1}{2\pi i} \int_0^{2\pi} dk_m \partial_{k_m} \ln \det \left[E + \sum_{\mathbf{j}} t_{\mathbf{j}}^* e^{\mathbf{j} \cdot (\boldsymbol{\mu} + i\mathbf{k})} \right] \\
&= \frac{1}{2\pi i} \int_0^{2\pi} dk_m \partial_{k_m} \ln \det \left[-E - \sum_{\mathbf{j}} t_{\mathbf{j}}^* e^{\mathbf{j} \cdot (\boldsymbol{\mu} + i\mathbf{k})} \right] \\
&= \frac{-1}{2\pi i} \int_0^{2\pi} dk_m \partial_{k_m} \ln \det \left[-E^* - \sum_{\mathbf{j}} t_{\mathbf{j}} e^{\mathbf{j} \cdot (\boldsymbol{\mu} - i\mathbf{k})} \right] \\
&= \frac{1}{2\pi i} \int_0^{2\pi} dk_m \partial_{k_m} \ln \det \left[-E^* - \sum_{\mathbf{j}} t_{\mathbf{j}} e^{\mathbf{j} \cdot (\boldsymbol{\mu} + i\mathbf{k})} \right] \\
&= \frac{1}{2\pi i} \int_0^{2\pi} dk_m \partial_{k_m} \ln \det [-E^* - H(e^{\boldsymbol{\mu} + i\mathbf{k}})].
\end{aligned} \tag{S34}$$

Thus, $\tilde{E}_{\mathcal{T}_-} = -E^*$, $\tilde{\boldsymbol{\mu}}_{\mathcal{T}_-} = \boldsymbol{\mu}$.

SLS

$$\begin{aligned}
w_m^\Gamma(E) &= \frac{1}{2\pi i} \int_0^{2\pi} dk_m \partial_{k_m} \ln \det \left[E - \sum_{\mathbf{j}} U_\Gamma t_{\mathbf{j}} U_\Gamma^{-1} e^{\mathbf{j} \cdot (\boldsymbol{\mu} + i\mathbf{k})} \right] \\
&= \frac{1}{2\pi i} \int_0^{2\pi} dk_m \partial_{k_m} \ln \det \left[E + \sum_{\mathbf{j}} t_{\mathbf{j}} e^{\mathbf{j} \cdot (\boldsymbol{\mu} + i\mathbf{k})} \right] \\
&= \frac{1}{2\pi i} \int_0^{2\pi} dk_m \partial_{k_m} \ln \det \left[-E - \sum_{\mathbf{j}} t_{\mathbf{j}} e^{\mathbf{j} \cdot (\boldsymbol{\mu} + i\mathbf{k})} \right] \\
&= \frac{1}{2\pi i} \int_0^{2\pi} dk_m \partial_{k_m} \ln \det [-E - H(e^{\boldsymbol{\mu} + i\mathbf{k}})].
\end{aligned} \tag{S35}$$

Thus, $\tilde{E}_\Gamma = -E$, $\tilde{\boldsymbol{\mu}}_\Gamma = \boldsymbol{\mu}$.

Pseudo Hermitian Symmetry

$$\begin{aligned}
w_m^\eta(E) &= \frac{1}{2\pi i} \int_0^{2\pi} dk_m \partial_{k_m} \ln \det \left[E - \sum_{\mathbf{j}} \eta t_{\mathbf{j}} \eta^{-1} e^{\mathbf{j} \cdot (\boldsymbol{\mu} + i\mathbf{k})} \right] \\
&= \frac{1}{2\pi i} \int_0^{2\pi} dk_m \partial_{k_m} \ln \det \left[E - \sum_{\mathbf{j}} t_{-\mathbf{j}}^\dagger e^{\mathbf{j} \cdot (\boldsymbol{\mu} + i\mathbf{k})} \right] \\
&= \frac{1}{2\pi i} \int_0^{2\pi} dk_m \partial_{k_m} \ln \det \left[E - \sum_{\mathbf{j}} t_{\mathbf{j}}^* e^{\mathbf{j} \cdot (-\boldsymbol{\mu} - i\mathbf{k})} \right] \\
&= \frac{-1}{2\pi i} \int_0^{2\pi} dk_m \partial_{k_m} \ln \det \left[E^* - \sum_{\mathbf{j}} t_{\mathbf{j}} e^{\mathbf{j} \cdot (-\boldsymbol{\mu} + i\mathbf{k})} \right] \\
&= \frac{-1}{2\pi i} \int_0^{2\pi} dk_m \partial_{k_m} \ln \det [E^* - H(e^{-\boldsymbol{\mu} + i\mathbf{k}})].
\end{aligned} \tag{S36}$$

Thus, $\tilde{E}_\eta = E^*$, $\tilde{\boldsymbol{\mu}}_\eta = -\boldsymbol{\mu}$.

Now, we get the results in table I in main text.

EXAMPLES

PHS

We consider a 2-dimensional non-Hermitian system with PHS, the Hamiltonian under PBC is

$$H_{PHS}(k_x, k_y) = \begin{pmatrix} m + i\gamma + t_x e^{ik_x} + t_y e^{ik_y} & t \\ \tilde{t} & -m - i\gamma - t_x e^{ik_x} - t_y e^{ik_y} \end{pmatrix}. \tag{S37}$$

The operator of PHS is

$$\hat{C}_- = U_{C_-} = \begin{pmatrix} 0 & 1 \\ -1 & 0 \end{pmatrix}. \tag{S38}$$

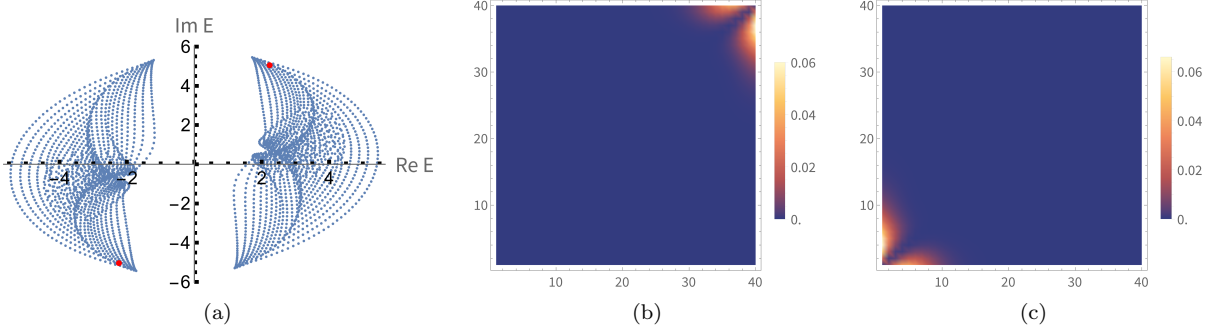


FIG. 4. (a) The blue dots are the spectrum of the system given by Eq.(S37) under OBC. Two red dots are $E_{PHS1} = 2.24 + 5.05i$ and $E_{PHS2} = -2.24 - 5.05i$ respectively. (b) The distribution of wave function corresponding to E_{PHS1} . (c) The distribution of wave function corresponding to E_{PHS2} . Values of parameters are $m = 1.5$, $\gamma = 1$, $t_x = 3$, $t_y = 2.5$, $t = 1$, $\tilde{t} = 2$. The size of the system is 40×40 .

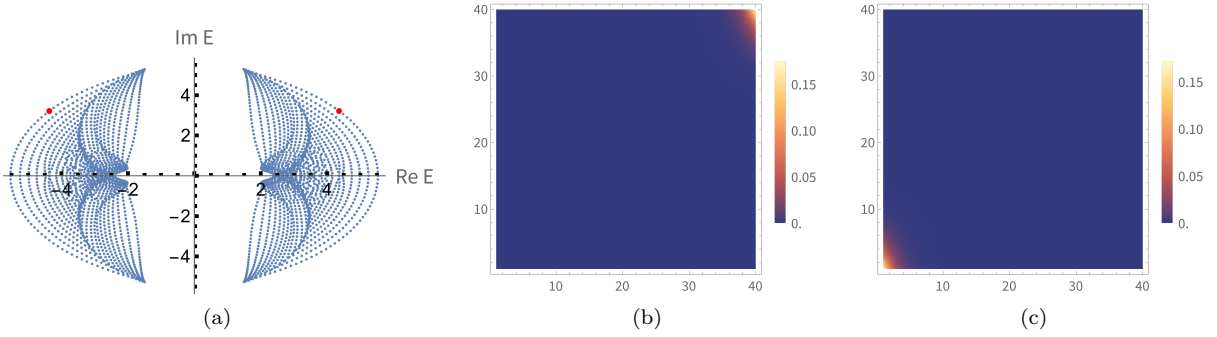


FIG. 5. (a) The blue dots are the spectrum of the system given by Eq.(S39) under OBC. Two red dots are $E_{CS1} = 4.36 + 3.21i$ and $E_{CS2} = -4.36 + 3.21i$ respectively. (b) The distribution of wave function corresponding to E_{CS1} . (c) The distribution of wave function corresponding to E_{CS2} . Values of parameters are $m = 1.5$, $t_x = 3$, $t_y = 2.5$, $t = 1$, $\tilde{t} = 2$. The size of the system is 40×40 .

The spectrum under OBC for specific values of parameters are given in Fig.4. For two eigenenergies, $E_{PHS1} = 2.24 + 5.05i$ and $E_{PHS2} = -2.24 - 5.05i$, belong to the OBC spectrum, $E_{PHS1} = -E_{PHS2}$ and eigenstates corresponding to them are localized at the opposite boundary.

CS

Setting $\gamma = 0$ in Eq.(S37), the Hamiltonian given in Eq.(S37) has TRS. Thus, we take the Hamiltonian with CS under PBC as

$$H_{CS}(k_x, k_y) = \begin{pmatrix} m + t_x e^{ik_x} + t_y e^{ik_y} & t \\ \tilde{t} & -m - t_x e^{ik_x} - t_y e^{ik_y} \end{pmatrix}, \quad (\text{S39})$$

and the operator of CS is

$$\hat{S} = U_S K = \begin{pmatrix} 0 & 1 \\ -1 & 0 \end{pmatrix} K. \quad (\text{S40})$$

We still take values of the parameters as $m = 1.5$, $t_x = 3$, $t_y = 2.5$, $t = 1$, $\tilde{t} = 2$. In this case, for two eigenenergies, $E_{CS1} = 4.36 + 3.21i$ and $E_{CS2} = -E_{CS1}^* = -4.36 + 3.21i$, eigenstates corresponding to E_{CS1} and E_{CS2} are localizing at the opposite boundary (See Fig.5).

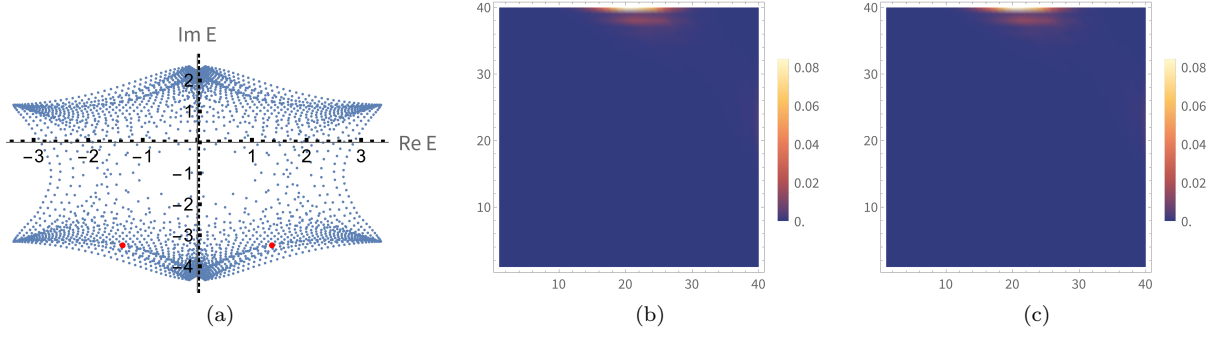


FIG. 6. (a) The blue dots are the spectrum of the system given by Eq.(S41) under OBC. Two red dots are $E_{PHS^\dagger 1} = 1.37 - 3.33i$ and $E_{PHS^\dagger 2} = -1.37 - 3.33i$ respectively. (b) The distribution of wave function corresponding to $E_{PHS^\dagger 1}$. (c) The distribution of wave function corresponding to $E_{PHS^\dagger 2}$. Values of parameters are $\tilde{t}_0 = -1$, $t_0 = 3$, $t_x = 2$, $t_y = 2.3$, $\gamma = 2$. The size of the system is 40×40 .

PHS[†]

Consider the 2-dimensional non-Hermitian Hamiltonian under PBC,

$$H_{PHS^\dagger}(k_x, k_y) = \begin{pmatrix} \tilde{t}_0 + t_x e^{-ik_x} + t_y e^{-ik_y} & t_0 + t_x e^{-ik_x} + t_y e^{-ik_y} \\ i\gamma & -2i\gamma \end{pmatrix}. \quad (\text{S41})$$

This system has PHS[†] and the operator of PHS[†] is

$$\hat{\mathcal{T}}_- = U_{\mathcal{T}_-} = \begin{pmatrix} 1 & 0 \\ 0 & -1 \end{pmatrix}. \quad (\text{S42})$$

The spectrum under OBC is given in Fig.6. Eigenstate corresponding to $E_{PHS^\dagger 1} = 1.37 - 3.33i$ is localized at the same boundary with the eigenstate corresponding to $E_{PHS^\dagger 2} = -E_{PHS^\dagger 1}^* = -1.37 - 3.33i$.

SLS

We consider the non-Hermitian system with SLS, whose Hamiltonian under PBC is

$$H_\Gamma(k_x, k_y) = \begin{pmatrix} 0 & t_0 + m + i\gamma_1 + t_{-1} e^{-ik_x} + w_{-1} e^{-ik_y} \\ t_0 - m + i\gamma_2 + t_1 e^{ik_x} + w_1 e^{ik_y} & 0 \end{pmatrix}, \quad (\text{S43})$$

and the operator of SLS is

$$\hat{\Gamma} = U_\Gamma K = \begin{pmatrix} 1 & 0 \\ 0 & -1 \end{pmatrix} K. \quad (\text{S44})$$

The OBC spectrum under specific values of parameters are shown in Fig.7. Two eigenstates corresponding to $E_{\Gamma 1} = -4.87 + 0.70i$ and $E_{\Gamma 2} = -E_{\Gamma 1} = 4.87 - 0.70i$ respectively are localized at the same boundary.

Pseudo Hermitian Symmetry

Consider a non-Hermitian system with pseudo Hermitian symmetry, whose Hamiltonian under PBC is

$$H_\eta(k_x, k_y) = \begin{pmatrix} t_0 + i\gamma + t_{-1} e^{-ik_x} + t_1 e^{ik_x} & m_1 + w e^{-ik_y} + w e^{ik_y} \\ m_2 + w e^{-ik_y} + w e^{ik_y} & t_0 - i\gamma + t_{-1} e^{ik_x} + t_1 e^{-ik_x} \end{pmatrix}, \quad (\text{S45})$$

and the operator of pseudo Hermitian symmetry is

$$\hat{\eta} = U_\eta = \begin{pmatrix} 0 & 1 \\ 1 & 0 \end{pmatrix}. \quad (\text{S46})$$

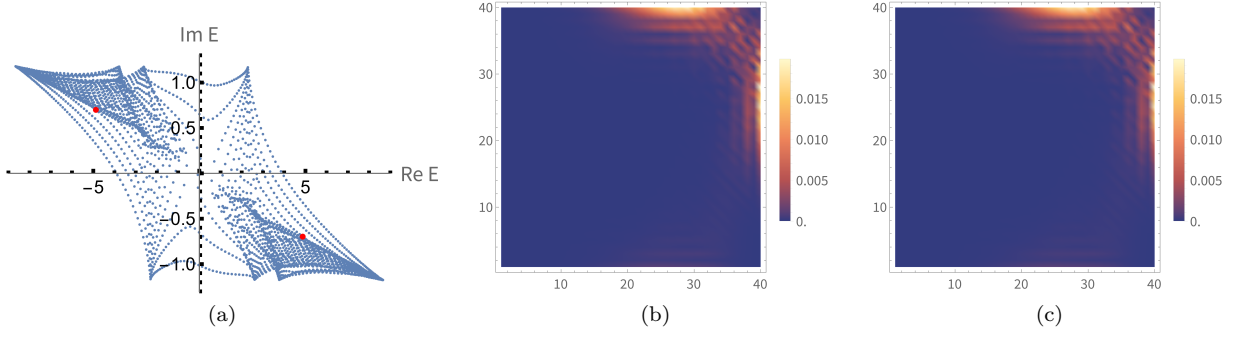


FIG. 7. (a) The blue dots are the spectrum of the system given by Eq.(S43) under OBC. Two red dots are $E_{\Gamma_1} = -4.87 + 0.70i$ and $E_{\Gamma_2} = 4.87 - 0.70i$ respectively. (b) The distribution of wave function corresponding to E_{Γ_1} . (c) The distribution of wave function corresponding to E_{Γ_2} . Values of parameters are $t_0 = 3$, $m = 1.5$, $\gamma_1 = 1$, $\gamma_2 = -2$, $t_1 = 2$, $t_{-1} = 3$, $w_1 = 2.3$, $w_{-1} = 4$. The size of the system is 40×40 .

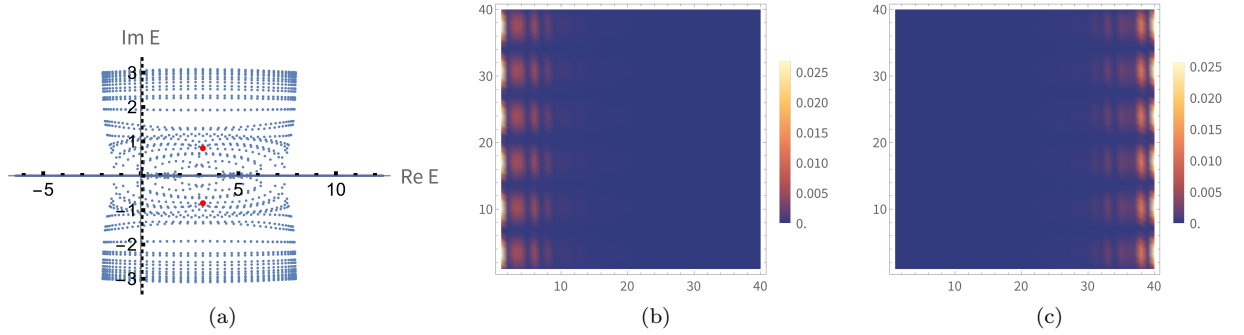


FIG. 8. (a) The blue dots are the spectrum of the system given by Eq.(S45) under OBC. Two red dots are $E_{\eta_1} = 3.19 + 0.80i$ and $E_{\eta_2} = 3.19 - 0.80i$ respectively. (b) The distribution of wave function corresponding to E_{η_1} . (c) The distribution of wave function corresponding to E_{η_2} . Values of parameters are $t_0 = 3$, $\gamma = 2$, $m_1 = 1.5$, $m_2 = -3$, $t_1 = 2$, $t_{-1} = 3$, $w = 2.3$. The size of the system is 40×40 .

The OBC specific of this system under specific values of parameters is shown in Fig.8. In this system, the eigenstate corresponding to $E_{\eta_1} = 3.19 + 0.80i$ and the eigenstate corresponding to $E_{\eta_2} = E_{\eta_1}^* = 3.19 - 0.80i$ are localized at the opposite boundary.

EXAMPLES OF BIDIRECTIONAL SKIN EFFECT IN A 2-DIMENSIONAL NON-HERMITIAN SYSTEM

In this section, we give examples of bidirectional skin effect in a 2-dimensional non-Hermitian system with TRS^\dagger . Consider such a model, whose Hamiltonian under PBC is

$$H_{\text{TRS}^\dagger}(k_x, k_y) = \begin{pmatrix} t_{-1}e^{-ik_x} + t_1e^{ik_x} + w_{-1}e^{-ik_y} + w_1e^{ik_y} & \gamma \\ \gamma & t_{-1}e^{ik_x} + t_1e^{-ik_x} + w_{-1}e^{ik_y} + w_1e^{-ik_y} \end{pmatrix}. \quad (\text{S47})$$

The operator of TRS^\dagger of this system is

$$\hat{C}_+ = U_{C_+} K = \begin{pmatrix} 0 & 1 \\ 1 & 0 \end{pmatrix} K. \quad (\text{S48})$$

Here, we take $t_1 = 1$, $t_{-1} = 3$, $w_1 = 1$, $w_{-1} = 2$. For $\gamma = 0$, there are two eigenstates degenerated at the same eigenenergy and localized at opposite boundary (Fig.9). For $\gamma = 0.1$, the degeneration disappears and bidirectional skin modes appear in the system (Fig.10). Then, we consider the case, $\gamma = 2$. In this case, the system has bidirectional skin mode and extended mode simultaneously (Fig.11).

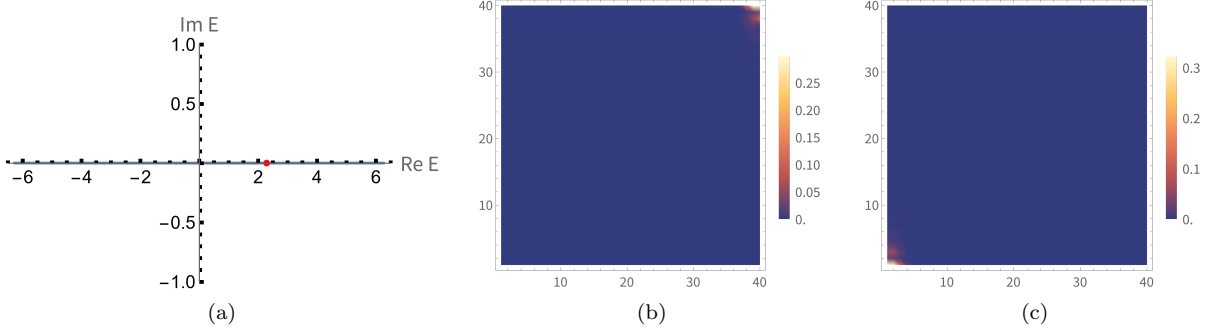


FIG. 9. (a)The blue line is the spectrum of the system given by Eq.(S47) under OBC for the case $\gamma = 0$. The red dot is $E_1 = 2.29$. (b) and (c) are distributions of two eigenstates degenerate at E_1 . The size of the system is 40×40 .

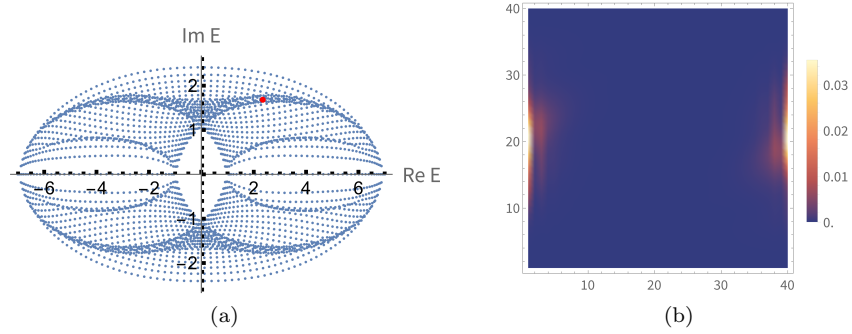


FIG. 10. (a)The blue dots are the spectrum of the system given by Eq.(S47) under OBC for the case $\gamma = 0.1$. The red dot is $E_2 = 2.35 + 1.68i$. (b) is the distribution of eigenstate corresponding to E_2 . The size of the system is 40×40 .

The two bands of $H_{TRS^\dagger}(k_x, k_y)$ are

$$E_{\pm}(k_x, k_y) = (t_1 + t_{-1}) \cos(k_x) + (w_1 + w_{-1}) \cos(k_y) \pm \sqrt{\gamma^2 - [(t_1 - t_{-1}) \sin(k_x) + (w_1 - w_{-1}) \sin(k_y)]^2}. \quad (\text{S49})$$

$E_{\pm}(k_x, k_y)$ are related by TRS^\dagger . Hence, according to the main text, the winding numbers of the two bands about E satisfy

$$w_x^{(+)}(E, k_y) = -w_x^{(-)}(E, k_y) \quad w_y^{(+)}(E, k_x) = -w_y^{(-)}(E, k_x). \quad (\text{S50})$$

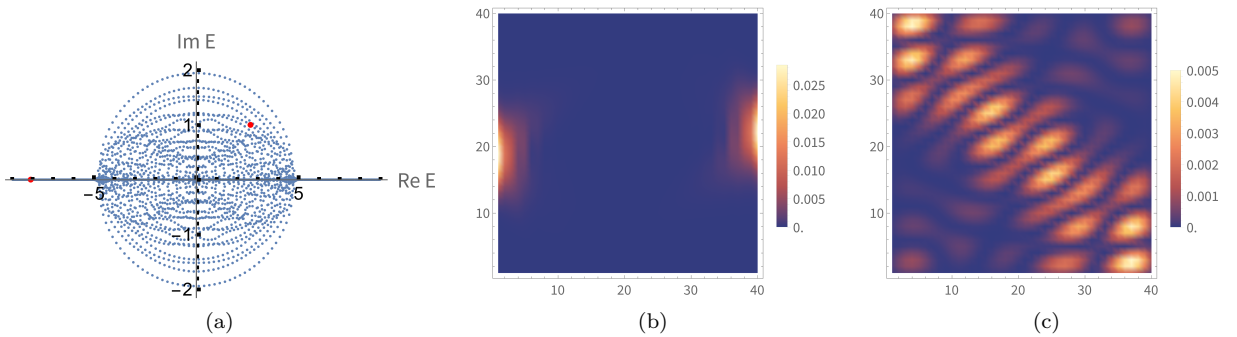


FIG. 11. (a)The blue dots are the spectrum of the system given by Eq.(S47) under OBC for the case $\gamma = 2$. The red dots are $E_3 = 2.65 + i$ and $E_4 = -8.09$. (b) and (c) are distributions of two eigenstates corresponding to E_3 and E_4 respectively. The size of the system is 40×40 .

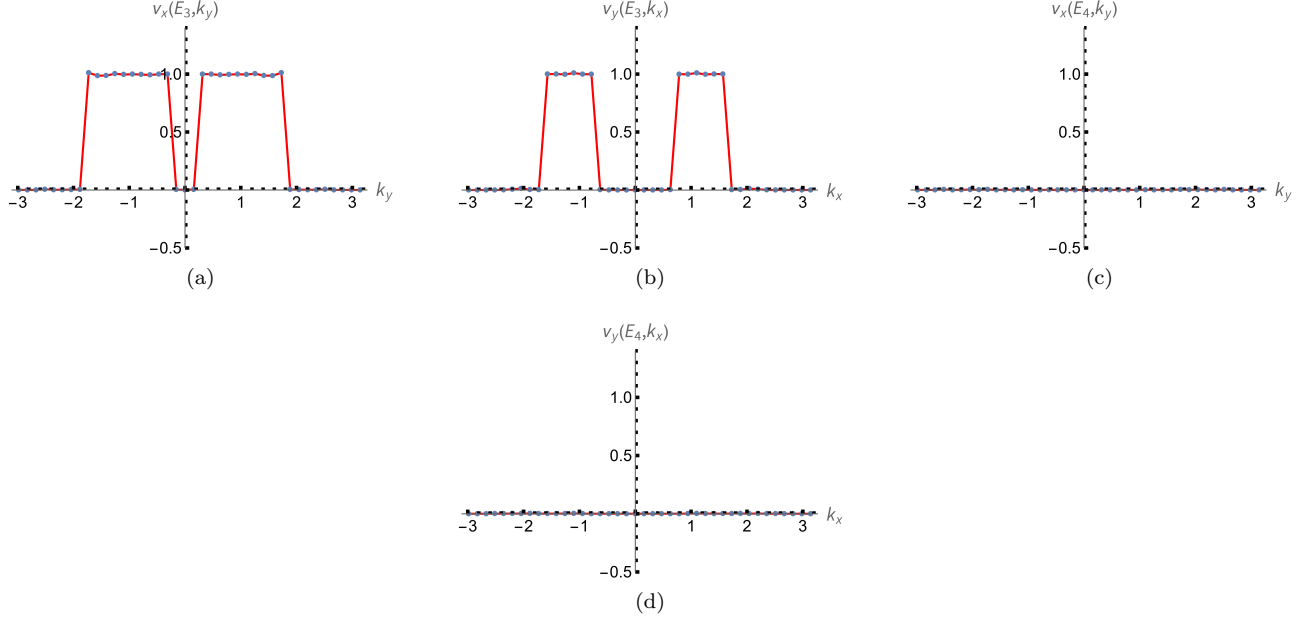


FIG. 12. The blue dots in (a), (b), (c) and (d) are values of $\nu_x(E_3, k_y)$, $\nu_y(E_3, k_x)$, $\nu_x(E_4, k_y)$ and $\nu_y(E_4, k_x)$ respectively for $k_x \in [-\pi, \pi]$ or $k_y \in [-\pi, \pi]$ in the case that $\gamma = 2$.

Then, according to Eq.(29) in the main text,

$$\nu_x(E, k_y) = |w_x^{(+)}(E, k_y)| \quad \nu_y(E, k_x) = |w_y^{(+)}(E, k_x)|. \quad (\text{S51})$$

For $\gamma = 2$, values of the topological invariants, $\nu_x(E, k_y)$ and $\nu_y(E, k_x)$ for $E = E_3$ and $E = E_4$ are given in Fig.12. For E_3 , the eigenstate corresponding to it is bidirectional skin mode and $\nu_x(E_3, k_y)$ and $\nu_y(E_3, k_x)$ can be non-zero for some values of k_x and k_y . For E_4 , the eigenstate corresponding to it is extended and $\nu_x(E_4, k_y) = \nu_y(E_4, k_x) = 0$ for all $k_x, k_y \in [-\pi, \pi]$. This is consistent with our conclusion in the main text.